VEGF-C expressing Tumor Associated Macrophages decrease hematogenous metastatic dissemination and normalizes the tumor vasculature

Sabrina de Souza Ferreira[1], Tatjana Wallmann[1*], Thomas Kerzel[2*], Majken Wallerius[1], Nele Schauer[1], Laura-Sophie Landwehr[1], Dennis Alexander Agardy[1], Jonas Bergh[1], Margarita Bartish[1,4], Johan Hartman[1,3], Mario Leonardo Squadrito[2°] and Charlotte Rolny[1°#].

[1]Karolinska Institute, Department of Oncology-Pathology, SciLifeLab, Stockholm, Sweden.
[2]San Raffaele Telethon Institute for Gene Therapy (TIGET), Universitá Vita-Salute San Raffaele, Milan, Italy.
[3]Department of Clinical Pathology and Cytology, Karolinska University Laboratory, Stockholm, Sweden.
[4]Gerald Bronfman Department of Oncology, Segal Cancer Centre, Lady Davis Institute and Jewish General Hospital, McGill University, Montreal, Quebec, Canada

*Equal Contribution
° Equal Contribution
[#]Corresponding author: Charlotte Rolny, Karolinska Institutet, Department of Oncology-Pathology, SciLifeLab, Solna 171 76 Stockholm, Phone: +46(0)8-517 76 882, e-mail: charlotte.rolny@ki.se

Running Title: VEGF-C normalizes the tumor vasculature

Keywords: Vascular Endothelial Growth Factor-C, Tumor-Associated Macrophages, Hypoxia, Vascular normalization, hematogenous cancer cell spreading, lymph node metastases.

Conflicts of interest: JH obtained speaker's honoraria or advisory board remunerations from Roche, Novartis, AstraZeneca, Eli Lilly. None of the other authors have a conflict of interest to disclose.

Total number of words: 6590; Figures: 4

ABSTRACT

Expression of pro-lymphangiogenic vascular endothelial growth factor C (VEGF-C) in primary tumors correlates with the occurrence of proximal lymph node metastasis in most solid cancer types. However, the role of VEGF-C in regulating tumor cell dissemination to distant organs is currently unclear. Perivascular tumor-associated macrophages (TAMs) are key regulators of hematogenous cancer cell spreading, forming tumor microenvironment of metastasis (TMEM) doorways for breast cancer cells to intravasate tumor blood vessels and fuel distant metastases. Using an experimental breast cancer (BC) model, we show here that TAMs expressing VEGF-C decrease cancer cell dissemination to the lung while enhancing lymph node metastasis. These TAMs express podoplanin and LYVE-1 and associate with normalized tumor blood vessels expressing VEGFR3. Further clinical data reveal that VEGF-C$^+$ TAMs correlate inversely with malignant grade and with the occurrence of TMEM complexes in a cohort of BC patients. Thus, our study displays an apparently paradoxical role of TAM-derived VEGF-C in redirecting cancer cells to preferentially disseminate to the lymph nodes, at least in part, by normalizing tumor blood vessels.

INTRODUCTION

Breast cancer (BC) is one of the most prevalent cancers worldwide (Waks and Winer, 2019). While the prognosis for non-macrometastatic BC is generally good due to availability of efficient adjuvant therapies, including targeted and endocrine therapy, the prognosis for metastatic BC or triple-negative breast cancer (TNBC) is worse partly due to resistance to therapy. New treatment strategies and prognostic biomarkers for these patients are therefore required.

VEGF-C promotes tumor lymphangiogenesis via its receptor VEGFR3, facilitating cancer cell dissemination to the sentinel lymph nodes (Tacconi et al., 2015). Even though the occurrence of metastases in tumor-draining lymph nodes is associated with poor clinical outcomes for many solid cancers, including BC (Dieterich and Detmar, 2016), it is still unclear to what extent metastatic seeding to lymph nodes further fuels pulmonary cancer cell colonization (Ma et al., 2018; Petrova and Koh, 2020). Experimental models of melanoma and mammary carcinoma suggest that a fraction of cancer cells populating lymph nodes do invade lymph node blood vessels, enter the blood stream circulation and colonize the lung (Brown et al., 2018; Pereira et al., 2018). On the other hand, by performing genetic analyses of clonal evolution between the primary tumor, lymph node metastases, and distant metastases of BC patients, we showed that cancer cells residing at distant sites stem from the primary tumor and

not from the sentinel lymph nodes (Ullah et al., 2018), suggesting that BC cells disseminate mainly via the hematogenous route to colonize distant organs.

Abnormal expression of VEGF-A results in atypical tumor vessels that are usually irregular, disorganized, permeable, and leaky, thus facilitating cancer cell intravasation into blood vessels (Goel et al., 2012). In contrast, normalization of the tumor vasculature is characterized by enhanced vessel perfusion, reduced tumor hypoxia and increased pericyte coating, resulting in hampering of distant metastasis (Mazzone et al., 2009). Perivascular tumor associated-macrophages (TAMs) are a major source of VEGF-A, and act as "doorways" for cancer cells to intravasate blood vessels (Harney et al., 2015). Indeed, TAMs play a key role in micro-anatomical structures termed tumor microenvironment of metastasis (TMEM), which are associated with increased occurrence of metastasis and are composed of a cancer cell (expressing the actin-regulatory protein mammalian-enabled, MENA), a perivascular TAM and an endothelial cell (Rohan et al., 2014). The density of TMEM assemblies has been shown to correlate with the occurrence of distant metastases in experimental mammary tumor models (Harney *et al.*, 2015) and BC patients (Ginter et al., 2019; Karagiannis et al., 2017; Rohan *et al.*, 2014). For this reason, strategies such as reprograming TAMs from a pro-angiogenic to an angiostatic state (Rolny et al., 2011) or impairing their association to blood vessels (Mazzieri et al., 2011) have been indicated as promising anti-metastatic intervention (Mazzieri *et al.*, 2011; Rolny *et al.*, 2011).

Building on the fact that TAMs are key players in BC metastatic dissemination, we investigated which TAM-derived factors could regulate the route of metastatic dissemination. We found that TAMs derived from a mammary tumor model preferentially disseminating via the lymphatic route expressed higher levels of VEGF-C as compared to TAMs isolated from a tumor mode that preferentially disseminated via the hematogenous route. In turn, forced overexpression of VEGF-C in TAMs regulate the localization and number of distant metastases by switching the route of metastatic dissemination from hematogenous to lymphatic. The mechanism whereby TAMs expressing VEGF-C hampered pulmonary metastasis was ascribed to augmented VEGFR3 expression on tumor vessels and was associated with increased vessel normalization and functionality. These data were substantiated in a cohort of ER^+ BC patients, showing that VEGF-C expressing TAMs correlated inversely with BC malignant grade and TMEM assembly. In summary, we propose a mechanism whereby TAM-derived VEGF-C attenuates pulmonary metastasis through mediating vascular normalization and is associated with increased VEGFR3 expression in tumor blood vessels and reprogramming of TAMs, both hampering cancer cell intravasation.

RESULTS

VEGF-C is highly expressed in TAMs of 66cl4 tumors but not of 4T1 tumors

To elucidate whether TAMs control the route of metastatic dissemination of cancer cells, we employed two metastatic mammary cancer cell lines, 4T1 and 66cl4, which are derived from a single mouse mammary tumor cell type but exhibit different capabilities to spread to proximal and distant organs (Aslakson and Miller, 1992). Both cell lines display features of human TNBC, *i.e.* absence of estrogen and progesterone receptors, and amplification of *Erb-B2* (a gene homologous to Human Epidermal Growth Factor Receptor 2, *HER2*).

We (Casazza et al., 2011) and others (Aslakson and Miller, 1992) have previously shown that 4T1 cancer cells preferentially disseminate to the lungs, while the 66cl4 cancer cells favor the lymph nodes. To confirm our previous findings, 4T1 and 66cl4 cancer cells from lungs and lymph node metastases were dissociated to a single cell suspension and cultured in the presence of the selection drug 6-thioguanine, for which both 4T1 and 66cl4 cancer cells display resistance. These clonogenic assays showed that 66cl4 cancer cells formed more colonies from the lymph node compared to the lungs, while 4T1 cancer cells readily formed colonies from lungs and fewer colonies from the lymph nodes (**Figure 1A**), in line with previous reports of analogous experiments (Casazza *et al.*, 2011). These findings suggest that 66cl4 cancer cells were more numerous in lymph nodes, whereas 4T1 cancer cells were preferentially located in lungs.

To investigate the involvement of TAMs in regulating the cancer cell metastatic fate, F4/80^{+}TAMs were sorted from 4T1- and 66cl4-tumors using fluorescence-activated cell sorting and analyzed by using qPCR to measure the expression level of genes associated with lymphatic and blood vessel formation**.** We found that 66cl4-infiltrating TAMs displayed substantially increased expression of genes encoding for the lymphangiogenic molecule VEGF-C*,* podoplanin (PDPN*),* the lymphatic vessel endothelial hyaluronic acid receptor 1 (LYVE-1*)* and the angiostatic cytokine CXCL12 as compared to 4T1-infiltrating TAMs (**Figure 1B**). Even though PDPN and LYVE-1 are mainly expressed on lymphatic vessels, it has recently been revealed that PDPN-expressing TAMs drive lymphangiogenesis and lymph endothelial intravasation (Bieniasz-Krzywiec et al., 2019), while LYVE 1-expressing TAMs maintain arterial homeostasis (Lim et al., 2018) and tumor angiogenesis (Opzoomer et al., 2021). Instead, 4T1-infiltrating TAMs exhibited higher expression levels of genes encoding for the pro-angiogenic molecules VEGFA and placental growth factor (PLGF) (**Figure 1B**). Further analysis by using immunofluorescence microscopy of tumor sections showed that the majority

of 66cl4-infiltrating TAMs expressed VEGF-C (**Figure 1C and 1D**), LYVE-1 (**Figure 1E and 1F**), and PDPN (**Figure 1G and 1H**) as compared to 4T1-infiltrating TAMs. We next investigated if the abundance of VEGF-C$^+$ TAMs was associated with increased lymphangiogenesis by analyzing the expression of CD31, a marker of blood vessels, and VEGFR3, a marker of lymph vessels, in 4T1- and 66cl4-tumor sections. Indeed, the 66cl4 tumors displayed more lymph vessels (VEGFR3$^+$CD31$^-$) as compared to 4T1 tumors (**Figure 1I and 1J**). Unexpectedly, CD31$^+$ blood vessels in 66cl4 tumors expressed VEGFR3 to a higher extent than blood vessels in 4T1 tumors (**Figure 1K and 1L**). Even though VEGFR3 expression is mainly restricted to lymphatic vessels in the adult, its expression can be induced during pathological conditions such as tumorigeneses (Valtola et al., 1999), and wound healing (Paavonen et al., 2000). Furthermore increased expression of VEGFR3 on blood vessels during embryogenesis has been suggested to control vascular permeability (Heinolainen et al., 2017). In summary, TAMs derived from a mammary tumor model, which preferentially disseminates via the lymphatic route and gives rise preferentially to lymph node metastases as compared to pulmonary metastases, expressed higher levels of VEGF-C, PDPN and LYVE-1 in contrast to TAMs isolated from a tumor model, which preferentially disseminates via the hematogenous route and gives rise preferentially to pulmonary metastases.

4T1 infiltrating TAMs expressing VEGF-C hamper pulmonary metastases

Building on the findings shown above, we hypothesized that VEGF-C expression by TAMs could control the route whereby cancer cells spread. We therefore generated chimeric mice harboring haemopoietic cells, including TAMs, overexpressing VEGF-C. To this end, we transduced hematopoietic stem/progenitor cells (HSPCs) with lentiviral vectors (LVs), either empty (*Ctr*) or encoding for *Vegfc.* Transduced HSPCs were then transplanted into recipient mice (hereon denoted *Ctr* or *Vegfc* chimeric mice, respectively) that had undergone myeloablation by busulfan treatment (Lund et al., 2018). Upon hematopoietic reconstitution (*i.e.* after 6 weeks from HSPC transplantation), 4T1 cells were injected into the fat-pad of the chimeric mice (visualized in **Figure S1A**). We found an average of 2 integrated lentiviral vector copies per mouse genome in bone marrow (BM) cells from either *Ctr* or *Vegfc*-chimeric mice by using qPCR analysis (**Figure S1B**), corresponding to ~80 % of all 4T1-infiltrating TAMs expressing VEGF-C (**Figure 2A and 2B**). Of note, VEGF-C expression in immune cells apart from TAMs, defined as cells positive for the expression of the pan-hemopoietic marker CD45, and negative for the expression of the pan macrophage marker F4/80, was minor. By using western blot analysis, we confirmed VEGF-C protein expression *ex vivo* in bone marrow-derived macrophages (BMDMs) isolated from transplanted *Ctr* and *Vegfc*-chimeric mice (**Figure S1C**). Importantly, transduction of HSPCs with *Vegfc* LV did not affect *Vegfa* expression in BMDMs (**Figure S1D).**

Overexpression of VEGF-C in TAMs did not modify 4T1 tumor growth rate (**Figure 2C**) nor the final tumor burden (**Figure S1E**). Clonogenic assays of dissociated lymph nodes and lungs from *Vegfc*-chimeric mice implanted with 4T1 tumors, which preferentially give rise to lung metastases, showed increased cancer cell colonies from lymph nodes (**Figure 2D**) but reduced colonies from lungs (**Figure 2E**) or blood (**Figure S1F**) as compared to controls. In agreement with this finding, immunohistochemical analysis of MENA-expressing cancer cells in lungs from *Ctr*-and *Vegfc*-chimeric mice implanted with 4T1 tumors confirmed that overexpression of *Vegfc* in TAMs decreased the incidence of pulmonary metastasis compared to control (**Figure 2F**).

We next investigated if *Vegfc* overexpression by TAMs affected lymph and blood angiogenesis by analysing tumor sections from *Ctr* and *Vegfc*-chimeric mice stained for VEGFR3 and CD31. Enforced expression of *Vegfc* in TAMs increased the number of VEGFR3^{+}CD31^{-} lymph vessels **(Figure S1G and S1H)** as well as the expression of VEGFR3 in CD31^{+} blood vessels compared to controls (**Figure 2G and 2H).** Even though the CD31^{+} vessel area was decreased in *Vegfc* 4T1 tumors as compared to controls (**Figure 2I),** the number of vessels was unchanged (**Figure 2J**), which may suggest normalization of the vessels in the presence of TAM-derived VEGF-C. Moreover, enforced *Vegfc* expression increased the number of TAMs that expressed LYVE-1 (**Figure 2K and 2L**) and PDPN (**Figure 2M and 2N)**. In summary, these data show that VEGF-C induces a phenotypic reprogramming of TAMs, which is in part reflected by increased expression of LYVE-1 and PDPN. This phenotypic remodeling of TAMs was associated with increased lymphangiogenesis, increased VEGFR3 expression in blood vessels, and hampered pulmonary metastasis.

TAM-derived VEGF-C normalizes the tumor vasculature

Blood vessel normalization hampers cancer cell invasion and seeding of pulmonary metastases (Mazzone *et al.*, 2009; Rolny *et al.*, 2011), and is generally associated with improved vessel perfusion, increased pericyte coverage as well as decreased tumor hypoxia (Mazzone *et al.*, 2009; Rankin and Giaccia, 2016). 4T1 tumor-bearing *Ctr* and *Vegfc* chimeric mice were injected with FITC-conjugated lectin (which will only label vessels with a blood flow) or the hypoxic marker pimonidazole hydrochloride (PIMO), intravenously or intraperitoneally respectively. Sections of 4T1 tumors from *Vegfc* chimeric mice displayed a significantly higher number of lectin perfused blood vessels (**Figure 3A and 3B**) and reduced tumor hypoxia (**Figure 3C and 3D**) compared to controls. In line, the number of blood vessels that were covered with α-SMA and NG2 positive pericytes was augmented in *Vegfc*-tumors as compared to controls (**Figure 3E and 3F**). In agreement with the enforced genetic expression of *Vegfc*

in TAMs, the number of perivascular TAMs expressing VEGF-C in *Vegfc*-tumors was increased as compared to *Ctr*-tumors (**Figure S2A and S2B)**. These results suggest that VEGF-C expression by TAMs is associated with tumor blood vessel normalization.

To further investigate the effect of macrophage-derived VEGF-C on tumor vessels, we employed an *in vivo* cancer cell and BMDM co-mingling assay (outlined in **Figure S2C**). In this assay, BMDMs were transduced with either LVs to enforce VEGF-C expression (*Ctr* or *Vegfc* LVs) or LVs driving the expression of short hairpins targeting *Vegfc* (*shVegfc LVs*) and were mixed in matrigel with 4T1 cancer cells. Transduced BMDMs comingled with 4T1 cancer cells were then injected subcutaneously into syngeneic mice. Implants were harvested 8 days post-injection. Immunostaining revealed that *Vegfc*-expressing TAMs augment the fraction of vessels labeled with FITC-conjugated lectin (**Figure 3G and 3H**) and increased the expression of VEGFR3 (**Figure 3I and 3J**) in blood vessels. Conversely, *shVegfc*-TAMs reduced the number of functional vessels, according to lectin staining (**Figure 3G and 3H**), and decreased the fraction of vessels expressing VEGFR3 (**Figure 3I and 3J**). Moreover, tumor hypoxia was reduced by *Vegfc* -expressing TAMs compared to controls (**Figure 3K and 3L**), while *shVegfc*-TAMs increased tumor hypoxia (**Figure 3K and 3L**). In summary, VEGF-C^{-}expressing TAMs normalize blood vessels and increase vessel functionality. On the other hand, downregulation of VEGF-C reduced vessel normalization and functionality, implicating a key role of TAM-derived VEGF-C in tumor blood vessel normalization.

VEGF-expressing TAMs do not alter the tumor immune composition

Lymphatic vessels are extensively involved in regulating immune cell trafficking, which may affect tumor growth and metastatic dissemination (Petrova and Koh, 2020). We therefore investigated if TAM-derived VEGF-C affected the tumor immune landscape by employing flow cytometry analysis. VEGF-C overexpression in TAMs did not affect the fraction of immune cells infiltrating tumors, including CD11b^{+} myeloid cells (**Figure S3A**), CD11b^{+}F4/80^{+} TAMs (**Figure S3B**), Ly6G^{+} neutrophils (**Figure S3C**), Ly6C^{+} monocytes (**Figure S3D**), immunostimulatory (also known as M1-like TAMs) (**Figure S3E**) or immunosuppressive TAMs (also known as M2-like TAMs) (**Figure S3F**). Immunostimulatory TAMs were identified by high expression of F4/80^{+}, MHC class II, CD11c^{+}, CD80^{+}, CD86^{+} and MHC class I^{+} (**Figure S3E)** while immunosuppressive F4/80^{+} TAMs were identified by low expression of MHC class II or elevated levels of mannose receptor c-type 1 (MRC1) (**Figure S3F**). Moreover, TAM-driven VEGF-C did not affect the accumulation of T cells (neither total CD3^{+} T cells or CD4^{+} and CD8^{+} T cell subpopulations) or CD49b^{+} NK cells (**Figure S3G**). Furthermore, we found that *ex vivo* BMDMs engineered to express VEGF-C did not display altered expression levels of genes encoding for the immunostimulatory cytokines such as C-X-C motif ligand (CXCL)-9, -10 and

-11, interleukin-1a (IL1a), or immunosuppressive factors including IL10, arginase1 (ARG1), MRC1 and transforming growth factor (TGFβ), detected by qPCR (**Figure S3H**). Altogether, these observations indicate that TAM-derived VEGF-C does not alter the immune landscape of tumors as well as the immune activation or polarization status of TAMs. Hence, the differential metastatic behavior observed upon TAM-mediated VEGF-C expression may be attributed to a direct effect on tumor vessels.

The number of VEGF-C expressing TAMs inversely correlates to TMEM complexes and grade of malignancy in human breast cancer

Based on our experimental data, we speculated that perivascular TAMs expressing VEGF-C may promote vessel normalization in human tumors and, therefore, be more frequent in low-grade BC as compared to high-grade BC. The majority of available TNBC patient specimens belong to high-grade tumors (*i.e.* grade 3, where the cancer cells are poorly differentiated and undergo rapid proliferation), whereas for our study we needed a population of specimens comprising both low grade and high-grade tumors. Building on this, we focused on estrogen receptor (ER)-positive breast cancer, which is also the most prevalent type in BC patients (~70 %) and can be targeted with endocrine therapy. However, half of the treated patients will develop metastatic disease within 20-years of diagnosis. (Sheppard et al., 2014). Hence, we evaluated the accumulation of bulk and perivascular TAMs by immunostaining tumor sections from ER^+ BC patient specimens of different histological grades (Nottingham Histological Grade I-III, where grade I and II indicate low grade, and grade III accounts for high grade). Both the total amount of $CD68^+$ TAMs (**Figure 4A and 4B**) and perivascular TAMs (**Figure 4C**) accumulated to a higher extent in high-grade ER^+ BC as compared to low-grade ER^+ BC. Additional immunofluorescence staining, which also included VEGF-C, revealed that both bulk TAMs (**Figure 4D and 4E**) and perivascular TAMs **(Figure 4D and 4F)** expressed VEGF-C to higher levels in low-grade than in high-grade ER^+ BC.

As information for distant metastases for this patient cohort was not available, we evaluated the occurrence of TMEM assemblies, which is a clinically validated prognostic marker for the occurrence of distant metastasis in BC patients (Oktay et al., 2012; Robinson et al., 2009; Rohan *et al.*, 2014). Immunofluorescence staining of TMEM assemblies revealed that the TMEM score was increased in high-grade compared to low-grade ER^+ BC tumors (**Figure 4G and 4H**). Importantly, the TMEM score was inversely correlated with the presence of TAMs expressing VEGF-C (**Figure 4I**), and thus TAMs expressing VEGF-C may also inversely correlate with lung metastases. Altogether, these results suggest that VEGF-C expression by TAMs may play a key role in determining the preferential route of cancer cell seeding for distant metastases. Indeed, VEGF-C expression by TAMs may normalize tumor

vessels limiting cancer cell spreading through the hematogenous route favoring the lymphatic route. Thus, our work points out a new molecular mechanism by which TAMs may foster or limit lung metastases in BC and sets the ground for identifying new prognostic tools and designing targeted interventions aimed at interfering with the metastatic process.

DISCUSSION

TAMs are regulators of tumor progression and have been linked to poor clinical outcomes in most cancers (9-11). Like macrophages in many other tissues, TAMs show remarkable functional plasticity and often exhibit a spectrum of activation states that span from an immunostimulatory and anti-metastatic phenotype (sometimes referred to as M1-like) to an immunosuppressive and pro-metastatic phenotype (also referred to as M2-like) (Mantovani et al., 2017). Usually, TAMs will express markers characteristic of both activation states and their function will partly depend on their spatial localization (Yang et al., 2018). For instance, perivascular macrophages promote angiogenesis (De Palma et al., 2007) by secreting factors such as VEGF-A, which increases vessel permeability and favors cancer cell intravasation (Harney *et al.*, 2015; Karagiannis *et al.*, 2017). Perivascular TAMs are furthermore a part of the TMEM assembly that functions as gateways for hematogenous spreading (Entenberg et al., 2020; Ginter *et al.*, 2019; Harney *et al.*, 2015; Karagiannis *et al.*, 2017; Oktay *et al.*, 2012; Rohan *et al.*, 2014).

For the past decades it has been debated to what extend metastatic cancer cells in lymph nodes give rise to metastases in other distant organs, such as lungs, brain or liver; or whether distant metastases originate directly from the primary tumors or from circulating cancer cells (Petrova and Koh, 2020). As VEGF-C is the main factor stimulating lymphangiogenesis, it has been correlated to lymph node metastasis (Dieterich and Detmar, 2016). VEGF-C stimulates lymphangiogenesis via activation of VEGFR3 but can also regulate angiogenesis by binding to VEGFR2/VEGFR3 heterodimers, expressed by blood vessels during embryogenesis, endothelial tip cells in adults and tumor blood vessels (Roy et al., 2006; Tammela et al., 2011). The role of VEGFR3 expression on blood vessels has been reported to maintain their maturation (Tammela *et al.*, 2011). In contrast, deletion of VEGFR3 in blood vessels enhances VEGFR2 expression that stimulates the VEGFA/VEGFR2 pathway, resulting in excessive angiogenesis in Lewis Lung Carcinoma (Tammela *et al.*, 2011). In our model, elevated levels of VEGF-C in TAMs increased VEGFR3 expression on tumor vessels, which is associated with better vessel functionality. In contrast, silencing of VEGF-C decreased VEGFR3 expression in blood vessels concomitant with vessel abnormalization. In line, Tammela and co-authors suggested that during postnatal vascular development VEGF-C expressing macrophages activates VEGFR-3 in the endothelial tip cells, leading to decreased sensitivity to the VEGF-

A, and fusion of the two tip cells to a mature vessel (Tammela *et al.*, 2011). Our data do not only suggest that VEGF-C expressing TAMs are key regulators of functional vascular development but also redirects cancer cells to disseminate via lymphatic vessels instead of the hematogenous route by also inducing expression of PDPN. In line, Bieniasz-Krzywiec and colleagues suggested that PDPN expression by TAMs facilitated extracellular matrix degradation promoting lymphoinvasion facilitating lymph node metastases (Bieniasz-Krzywiec *et al.*, 2019). Elevated levels of LYVE-1 expression on lymphatic endothelium is generally correlated to increased lymph angiogenesis (Ma *et al.*, 2018). Recently, Opzoomer et al., suggested that a subpopulation of perivascular TAMs that express LYVE-1 were especially pro-angiogenic (Opzoomer *et al.*, 2021). Here, we instead suggest that perivascular TAMs expressing a combination of VEGF-C, PDPN and LYVE-1 on one hand normalized the tumor vasculature and on the other hand facilitated lymphoinvasion by cancer cells. Further clinical relevance for VEGF-C-expressing TAMs in counteracting hematogenous metastatic dissemination was showed in a cohort of ER^+ BC specimens. Perivascular VEGF-C^+ TAMs correlated inversely with malignant grade and with the occurrence of TMEM complexes. Thus, even though VEGF-C levels in primary tumors and in serum correlate to malign tumors and lymph node metastases (Dieterich and Detmar, 2016; Petrova and Koh, 2020), these levels might just be an indicative of malign disease rather than VEGF-C itself fueling the occurrence of distant metastases. Collectively, our data show that TAM-derived VEGF-C plays an unexpected role in normalizing the tumor vasculature, redirecting cancer cells to preferentially spread to the lymph nodes and dampening pulmonary metastases. This study paves the way for future works aimed at dissecting the contribution of VEGF-C in seeding of distant metastases from other tumor types, as well as identifying new prognostic markers and designing new targeted interventions aimed at thwarting the metastatic process.

MATERIALS AND METHODS

Generation of the VEGF-C vector

Vegfc ORF clone was purchased from Thermo Scientific Fisher and amplified by PCR (95 °C for 5 min, 5 cycles at 95 °C for 30 sec, 45 °C for 30 sec, 72 °C for 30 sec and 30 cycles at 95 °C for 30 sec, 68 °C for 30 sec, 72 °C for 30 sec). Primers for *Vegfc* amplification are FW 5'-TAAAGACCGGTCAAAAGTTGCGAGCC-3' and RW 5'-TCGGGGTCGACTACAATTTTCATTTTATTTTAAAC-3' primers. The DNA coding for *Vegfc* was then inserted into a CMV.GFP.WPRE lentiviral vector sequence as described previously (Keklikoglou et al., 2019) downstream to the CMV promoter.

Lentivirus production

Vesicular stomatitis virus-G protein (VSV-G)-pseudotyped lentivirus vectors either empty or encoding *Vegfc* were produced by transient four-plasmid co-transfection into HEK293T cells and concentrated using ultracentrifugation as described previously (De Palma and Naldini, 2002a). Lentiviral vector titers were determined on HEK293T cells by TaqMan analysis as described previously (De Palma and Naldini, 2002b). Lentiviral vectors were resuspended in PBS and stored at -80 °C. shVEGF-C (NM 009506.2) lentiviral particles were bought from GeneCopeia (product number MSH028515).

Cell culture

Tumor cell lines

HEK293T cells were grown in Dulbecco's Modified Eagle's Medium (DMEM) while 66cl4 and 4T1 mammary carcinoma cells were grown in RPMI-1640 medium (Gibco). Both the RPMI-1649 and the DMEM mediums were supplemented with 10% fetal bovine serum, 1% penicillin/streptomycin (Gibco) and 1% L-glutamine (Gibco). 4T1 and 66cl4 mouse mammary carcinoma cells were originally derived from a single spontaneous tumor that arose in a BALB/cfC3H mouse and were purchased from the Karmanos Cancer Institute at Wayne State University.

Generation of 4T1 cells expressing VEGF-C

1 x 10^6 4T1 cells were transduced with 1 x 10^8 TU/ml of empty vector or *Vegfc* LVs in the presence of polybrene (SIGMA).

Bone-marrow derived macrophages (BMDMs)

Bone marrow cells were acquired by flushing the femurs and tibias of female BALB/c mice as described before(Bartish et al., 2020) (37). Cells were cultured in RPMI-1640 medium (Gibco) supplemented with 10% fetal bovine serum, 1% penicillin/streptomycin (Gibco), 1% L-glutamine (Gibco) and 50 ng/ml M-CSF (Miltenyi) for 8 days as described before (Bartish *et al.*, 2020).

gDNA isolation and quantitative RT-PCR

To evaluate the integration of the viral backbone into the hematopoietic progenitor cells, bone marrow of transplanted tumor bearing CTR and VEGF-C mice was isolated and gDNA was purified using QIAmp DNA Mini Kit (Qiagen) as described(De Palma et al., 2005) (37). Vector integration was determined by quantifying copy numbers of HIV normalized to housekeeping gene beta actin by quantitative RT-PCR (95 °C for 10min, 40 cycles at 95 °C for 15 sec and 60 °C for 1 min).

Quantitative PCR

Flow sorted 66cl4- and 4T1-tumor cells, 66cl4 and 4T1 infiltrating TAMs and BMDMs were collected in RLT buffer (Qiagen) and homogenized using a syringe with a 20G needle. RNA was extracted using the RNeasy Mini Kit (Qiagen) according to the manufacturer's instructions and reverse-transcribed with the QuantiTect Reverse Transcription kit according to the manufacturer's instructions (Qiagen). Genomic DNA was eliminated using gDNA Wipeout Buffer (Qiagen) for 2 min at 42 °C. qPCR was performed using either TaqMan Universal MasterMix II and TaqMan Gene Expression Assays (Applied Biosystems) or SYBR™ Green PCR Master Mix (Applied Biosystems) in a total volume of 10 µL. The polymerase was activated at 95 °C for 10 min and the PCR was performed for 40 cycles (95 °C for 15 s and 60 °C for 60 s). Following TaqMan probes for the following genes were used: *Vegfa* (Mm01281449_m1), *Vegfc* (Mm00437310_m1), *Cxcl9* (Mm00434946_m1), *Cxcl10* (Mm00445235_m1), *Cxcl11* (Mm00444662_m1), *Il10* (Mm00439614_m1), *Arginase1* (Mm00475988_m1), *Mrc1* (Mm01329362_m1), *Tgfβ* (Mm01178820_m1), *plgf* (Mm00435613_m1) podoplanin (Mm00494716_m1, LYVE-1 (Mm00475056_m1), CXCl12 Mm00445553_m1 and *β-actin* (Mm00607939_s1) all from Thermo Fisher Scientific .

Tumor experiments in mice

Female BALB/c mice (4-6 weeks old) were purchased from Charles River Laboratory. 2 x 10^5 4T1 cells were injected into the mammary fat pad of anesthetized animals. Tumor size was measured externally using calipers, and tumor volumes were estimated using the following equation: V_{sphere} = 4/3 π x (d/2) 2 x D/2 (d: minor tumor axis, D: major tumor axis). Mice were euthanized at maximum 1000 mm^3, and tumors were weighed after dissection. All ethical permits were obtained from the Swedish Board of Agriculture (N65/16 and 8525-2020).

Bone marrow transplant

Bone marrow cells were acquired by flushing the femurs and tibias of 6- to 8-week-old female BALB/c mice and treated with red blood cell lysis buffer (Sigma). Lineage negative hematopoietic stem and progenitor cells (HSPCs) were purified using EasySep Isolation Kit (StemCell Technologies) according to manufacturer's instructions. 2 x 10^6 lineage negative cells/ml were transduced with 1 x 10^8 TU/ml of empty vector or *Vegfc* lentivirus in serum-free StemSpan medium (StemCell Technologies) supplemented with 10 ng/ml IL-3, 20 ng/ml IL-6, 100 ng/ml SCF and 10 ng/ml FL-T3L (Stem Cell Technologies). 1 x 10^6 transduced HSPCs were resuspended in PBS and injected into the tail vein of 6-week-old female Balb/c mice, that had undergone myeloablation using 20 mg/kg Busulfan (Sigma) by intraperitoneal (i.p.)

injection on three consecutive days. Busulfan was solubilized in DMSO and diluted to 5 mg/ml in PBS. On the fourth day 12–14 × 10^6 BM cells were given by tail vein injection. This procedure resulted in ~80 % chimerism (Lund *et al.*, 2018).

Metastasis assay

Lungs and lymph nodes were dissected into an enzymatic buffer, dissociated to single cell suspensions and cultured in RPMI-1640 (complete medium) supplemented with 60 µM 6-Thioguanine (Sigma) as previously described (18) (Casazza *et al.*, 2011). Colonies formed by tumor cells resistant to 6-Thioguanine were fixed with 4 % Formaldehyde (VWR Chemicals) and stained with Hematoxylin Harris (VWR Chemicals). Metastasis colonies were counted, and the metastatic index was calculated by using the equitation M_{index} = n/w (n: number of metastases, w: weight of tumor)(Casazza *et al.*, 2011).

Flow Cytometry

Single cell suspensions tumors were pre-incubated with anti-CD16/32 mAb (BioLegend) for 15 min on ice to prevent non-specific binding, with subsequent incubation with specific antibodies for 30 min on ice. Cells were stained using the following antibodies: CD11b (M1/70), CD45 (30-F11), Ly6C (AL-21), Ly6G (1A8), CD86 (GL1), CD11c (HL3), CD3 (500A2/145-2c11), CD8 (53-6.7), CD4 (RM4-5), CD49b (HM ALPHA2), MHC class II (I-A/I-E), MHC class I (H-2K(d)) and CD80 (16-10A1; all from BD Bioscience), F4/80 (BM8) and MRC1 (C068C2; BioLegend). The viability of cells was verified using 7-AAD (Life Technologies). Samples were acquired with a LSR II (BD Biosciences) and analyzed using FlowJo software (Tree Star).

Co-mingling assay.

BMDM were transduced with 1 x 10^8 TU/ml of empty vector or *Vegfc* lentivirus vectors, 4 days post-differentiation. These transduced BMDMs were then embedded in 200 µL of growth factor reduced Matrigel (BD Bioscience) together with 2 × 10^5 4T1 tumor cells, 2 days after transduction, and injected subcutaneously into the flank of 8-week-old female BALB/c mice for 8 days.

Western Blot

Cells were lysed in NP-40 (Thermo Fisher Scientific) with freshly added Halt™ Protease Inhibitor Cocktail (Thermo Fisher Scientific). Protein concentrations were determined using the bicinchoninic acid (BCA) method (Thermo Fisher Scientific) according to the manufacturer's instructions. 20 µg of protein was incubated with antibodies against VEGF-C (Abd Serotec) for 2 h on ice before mixing with protein G-Sepharose (Thermo Fisher Scientific). The antibody

complex was washed three times in lysis buffer and once in Tris-buffered saline (TBS). The beads were resuspended in sample buffer, boiled for 5 min, and subjected to electrophoresis in 10% or 4–12% Bis-Tris gels and transferred to nitrocellulose membranes using iBlot2 (Life technologies). Membranes were probed for VEGF-C (Santa Cruz) followed by horseradish peroxidase-conjugated secondary antibodies (Life Technologies). Membranes were then washed and visualized with an enhanced chemiluminescence (ECL) detection system (GE Healthcare) and iBright CL1000 (Thermo Fisher Scientific). Signals were quantified using ImageJ software (NIH).

Immunofluorescence analysis

Tumors embedded in OCT, a cryo embedding matrix, were cut in 10 µm thick sections and fixed in methanol. Paraffin-embedded tumor sections were treated for antigen retrieval with sodium citrate buffer (Thermo Scientific Fisher). All tumor sections were blocked in blocking buffer containing PBS (Sigma), 0.3 % Triton X-100 (Sigma), 10 % fetal bovine serum (Gibco) and 1 % Bovine Serum Albumin (Sigma), and immunostained with the appropriate antibodies: anti CD68 (Dako), VEGFA (SantaCruz), CD31 (BD Biosciences), Podoplanin (Life Technologies), LYVE-1 (Medical and Biological Laboratories), NG2 (Merck Millipore), α-SMA (Sigma-Aldrich), F4/80 (Bio-Rad), VEGF-C (Santa Cruz), VEGFR3 (R&D Systems), CD31 (DAKO), FITC-Lectin (Bio-Rad) and MENA/ENAH (Sigma). The appropriate secondary antibodies were conjugated with AlexaFluor 488, AlexaFluor 546, AlexaFluor 555 or AlexaFluor 647 fluorochromes (Life Technologies). Cell nuclei were labeled with DAPI (Invitrogen Corp). 10 independent fields from each section were analyzed by using LSM 710 Zeiss confocal microscope and quantified by ImageJ software.

Tumor hypoxia and vessel functionality

Tumor hypoxia was assessed by intraperitoneal injection of 60 mg/kg pimonidazole hydrochloride (Hypoxiprobe) into tumor-bearing mice. Mice were sacrificed 1 h after injection and tumors were harvested. To detect the formation of hypoxic adducts, OCT tumor sections were immunostained with Hypoxyprobe-1-Mab-1 (Hypoxiprobe kit, Chemicon) following manufacturer's instructions. Vessel perfusion was evaluated by intravenous injection of 1 mg of FITC-conjugated Lectin (Molecular Probes). Tumors were embedded in OCT material (VWR Chemicals) and snap-frozen in iso-pentane (VWR Chemicals) on dry ice.

Patient material

Paraffin-embedded whole tumor sections from breast cancer patients were obtained from Karolinska University Hospital and Southern Hospital, Stockholm, Sweden. All breast cancer patients at the Karolinska University Hospital and Southern Hospital have approved and signed

a written consent for biobanking, including research purposes that have been approved by the local ethical committee (2016/957-31; *ex vivo* tumor models).

Statistical analysis

GraphPad Prism 6 software was used for graph/plot generation and statistical hypothesis testing. All data from representative experiments are presented with Standard Deviation (SD) and mean Statistical analyses were performed using Student's t-test, two-way ANOVA or one-way ANOVA as indicated in the figure legends. Stars and hashtags in the graphs indicate significance as depicted in the figure legends. Differences were considered statistically significant at $p<0.05$.

FINANCIAL SUPPORT

This study was supported by the Swedish Cancer Society (2016/825 and 2019/0281), Swedish Scientific Council (VR, 2018-02915 and 2021-01149), Radiumhemmets research funds (154352) to CR; Swedish Cancer Society and the Wallenberg foundation to JB; TW was supported by KI-PhD (2014-2018) foundation. JH was supported by grants from Radiumhemmets research funds, Swedish Breast Cancer Association, Swedish Society for Medical Research. MLS was supported by Fondazione Regionale per la Ricerca Biomedica (FRRB) 1751658-2020 and CARIPLO 1834-2019.

All the authors declare no conflict of interest regarding the work that is being submitted.

REFERENCES

Aslakson, C.J., and Miller, F.R. (1992). Selective events in the metastatic process defined by analysis of the sequential dissemination of subpopulations of a mouse mammary tumor. Cancer Res *52*, 1399-1405.

Bartish, M., Tong, D., Pan, Y., Wallerius, M., Liu, H., Ristau, J., de Souza Ferreira, S., Wallmann, T., van Hoef, V., Masvidal, L., et al. (2020). MNK2 governs the macrophage antiinflammatory phenotype. Proc Natl Acad Sci U S A. 10.1073/pnas.1920377117.

Bieniasz-Krzywiec, P., Martin-Perez, R., Ehling, M., Garcia-Caballero, M., Pinioti, S., Pretto, S., Kroes, R., Aldeni, C., Di Matteo, M., Prenen, H., et al. (2019). Podoplanin-Expressing Macrophages Promote Lymphangiogenesis and Lymphoinvasion in Breast Cancer. Cell Metab *30*, 917-936 e910. 10.1016/j.cmet.2019.07.015.

Brown, M., Assen, F.P., Leithner, A., Abe, J., Schachner, H., Asfour, G., Bago-Horvath, Z., Stein, J.V., Uhrin, P., Sixt, M., and Kerjaschki, D. (2018). Lymph node blood vessels provide exit routes for metastatic tumor cell dissemination in mice. Science *359*, 1408-1411. 10.1126/science.aal3662.

Casazza, A., Fu, X., Johansson, I., Capparuccia, L., Andersson, F., Giustacchini, A., Squadrito, M.L., Venneri, M.A., Mazzone, M., Larsson, E., et al. (2011). Systemic and targeted delivery of semaphorin 3A inhibits tumor angiogenesis and progression in mouse tumor models. Arterioscler Thromb Vasc Biol *31*, 741-749. 10.1161/ATVBAHA.110.211920.

De Palma, M., Murdoch, C., Venneri, M.A., Naldini, L., and Lewis, C.E. (2007). Tie2-expressing monocytes: regulation of tumor angiogenesis and therapeutic implications. Trends Immunol *28*, 519-524. S1471-4906(07)00245-1 [pii]

10.1016/j.it.2007.09.004.
De Palma, M., and Naldini, L. (2002a). Transduction of a gene expression cassette using advanced generation lentiviral vectors. Methods Enzymol *346*, 514-529.
De Palma, M., and Naldini, L. (2002b). Transduction of a gene expression cassette using advanced generation lentiviral vectors. Methods in enzymology *346*, 514-529.
De Palma, M., Venneri, M.A., Galli, R., Sergi Sergi, L., Politi, L.S., Sampaolesi, M., and Naldini, L. (2005). Tie2 identifies a hematopoietic lineage of proangiogenic monocytes required for tumor vessel formation and a mesenchymal population of pericyte progenitors. Cancer Cell *8*, 211-226.
Dieterich, L.C., and Detmar, M. (2016). Tumor lymphangiogenesis and new drug development. Adv Drug Deliv Rev *99*, 148-160. 10.1016/j.addr.2015.12.011.
Entenberg, D., Oktay, M.H., D'Alfonso, T., Ginter, P.S., Robinson, B.D., Xue, X., Rohan, T.E., Sparano, J.A., Jones, J.G., and Condeelis, J.S. (2020). Validation of an Automated Quantitative Digital Pathology Approach for Scoring TMEM, a Prognostic Biomarker for Metastasis. Cancers (Basel) *12*. 10.3390/cancers12040846.
Ginter, P.S., Karagiannis, G.S., Entenberg, D., Lin, Y., Condeelis, J., Jones, J.G., and Oktay, M.H. (2019). Tumor Microenvironment of Metastasis (TMEM) Doorways Are Restricted to the Blood Vessel Endothelium in Both Primary Breast Cancers and Their Lymph Node Metastases. Cancers (Basel) *11*. 10.3390/cancers11101507.
Goel, S., Wong, A.H., and Jain, R.K. (2012). Vascular normalization as a therapeutic strategy for malignant and nonmalignant disease. Cold Spring Harb Perspect Med *2*, a006486. 10.1101/cshperspect.a006486.
Harney, A.S., Arwert, E.N., Entenberg, D., Wang, Y., Guo, P., Qian, B.Z., Oktay, M.H., Pollard, J.W., Jones, J.G., and Condeelis, J.S. (2015). Real-Time Imaging Reveals Local, Transient Vascular Permeability, and Tumor Cell Intravasation Stimulated by TIE2hi Macrophage-Derived VEGFA. Cancer Discov *5*, 932-943. 10.1158/2159-8290.CD-15-0012.
Heinolainen, K., Karaman, S., D'Amico, G., Tammela, T., Sormunen, R., Eklund, L., Alitalo, K., and Zarkada, G. (2017). VEGFR3 Modulates Vascular Permeability by Controlling VEGF/VEGFR2 Signaling. Circ Res *120*, 1414-1425. 10.1161/CIRCRESAHA.116.310477.
Karagiannis, G.S., Pastoriza, J.M., Wang, Y., Harney, A.S., Entenberg, D., Pignatelli, J., Sharma, V.P., Xue, E.A., Cheng, E., D'Alfonso, T.M., et al. (2017). Neoadjuvant chemotherapy induces breast cancer metastasis through a TMEM-mediated mechanism. Sci Transl Med *9*. 10.1126/scitranslmed.aan0026.
Keklikoglou, I., Cianciaruso, C., Guc, E., Squadrito, M.L., Spring, L.M., Tazzyman, S., Lambein, L., Poissonnier, A., Ferraro, G.B., Baer, C., et al. (2019). Chemotherapy elicits pro-metastatic extracellular vesicles in breast cancer models. Nat Cell Biol *21*, 190-202. 10.1038/s41556-018-0256-3.
Lim, H.Y., Lim, S.Y., Tan, C.K., Thiam, C.H., Goh, C.C., Carbajo, D., Chew, S.H.S., See, P., Chakarov, S., Wang, X.N., et al. (2018). Hyaluronan Receptor LYVE-1-Expressing Macrophages Maintain Arterial Tone through Hyaluronan-Mediated Regulation of Smooth Muscle Cell Collagen. Immunity *49*, 1191. 10.1016/j.immuni.2018.12.009.
Lund, H., Pieber, M., Parsa, R., Han, J., Grommisch, D., Ewing, E., Kular, L., Needhamsen, M., Espinosa, A., Nilsson, E., et al. (2018). Competitive repopulation of an empty microglial niche yields functionally distinct subsets of microglia-like cells. Nat Commun *9*, 4845. 10.1038/s41467-018-07295-7.
Ma, Q., Dieterich, L.C., and Detmar, M. (2018). Multiple roles of lymphatic vessels in tumor progression. Curr Opin Immunol *53*, 7-12. 10.1016/j.coi.2018.03.018.
Mantovani, A., Marchesi, F., Malesci, A., Laghi, L., and Allavena, P. (2017). Tumour-associated macrophages as treatment targets in oncology. Nat Rev Clin Oncol *14*, 399-416. 10.1038/nrclinonc.2016.217.
Mazzieri, R., Pucci, F., Moi, D., Zonari, E., Ranghetti, A., Berti, A., Politi, L.S., Gentner, B., Brown, J.L., Naldini, L., and De Palma, M. (2011). Targeting the ANG2/TIE2 axis inhibits tumor growth and metastasis by impairing angiogenesis and disabling rebounds of proangiogenic myeloid cells. Cancer Cell *19*, 512-526. 10.1016/j.ccr.2011.02.005.

Mazzone, M., Dettori, D., Leite de Oliveira, R., Loges, S., Schmidt, T., Jonckx, B., Tian, Y.M., Lanahan, A.A., Pollard, P., Ruiz de Almodovar, C., et al. (2009). Heterozygous deficiency of PHD2 restores tumor oxygenation and inhibits metastasis via endothelial normalization. Cell *136*, 839-851. S0092-8674(09)00068-3 [pii]

10.1016/j.cell.2009.01.020.
Oktay, M.H., Gertler, F.B., Liu, Y.F., Rohan, T.E., Condeelis, J.S., and Jones, J.G. (2012). Correlated immunohistochemical and cytological assays for the prediction of hematogenous dissemination of breast cancer. J Histochem Cytochem *60*, 168-173. 10.1369/0022155411435153.
Opzoomer, J.W., Anstee, J.E., Dean, I., Hill, E.J., Bouybayoune, I., Caron, J., Muliaditan, T., Gordon, P., Sosnowska, D., Nuamah, R., et al. (2021). Macrophages orchestrate the expansion of a proangiogenic perivascular niche during cancer progression. Sci Adv *7*, eabg9518. 10.1126/sciadv.abg9518.
Paavonen, K., Puolakkainen, P., Jussila, L., Jahkola, T., and Alitalo, K. (2000). Vascular endothelial growth factor receptor-3 in lymphangiogenesis in wound healing. Am J Pathol *156*, 1499-1504. 10.1016/S0002-9440(10)65021-3.
Pereira, E.R., Kedrin, D., Seano, G., Gautier, O., Meijer, E.F.J., Jones, D., Chin, S.M., Kitahara, S., Bouta, E.M., Chang, J., et al. (2018). Lymph node metastases can invade local blood vessels, exit the node, and colonize distant organs in mice. Science *359*, 1403-1407. 10.1126/science.aal3622.
Petrova, T.V., and Koh, G.Y. (2020). Biological functions of lymphatic vessels. Science *369*. 10.1126/science.aax4063.
Rankin, E.B., and Giaccia, A.J. (2016). Hypoxic control of metastasis. Science *352*, 175-180. 10.1126/science.aaf4405.
Robinson, B.D., Sica, G.L., Liu, Y.F., Rohan, T.E., Gertler, F.B., Condeelis, J.S., and Jones, J.G. (2009). Tumor microenvironment of metastasis in human breast carcinoma: a potential prognostic marker linked to hematogenous dissemination. Clin Cancer Res *15*, 2433-2441. 1078-0432.CCR-08-2179 [pii]

10.1158/1078-0432.CCR-08-2179.
Rohan, T.E., Xue, X., Lin, H.M., D'Alfonso, T.M., Ginter, P.S., Oktay, M.H., Robinson, B.D., Ginsberg, M., Gertler, F.B., Glass, A.G., et al. (2014). Tumor microenvironment of metastasis and risk of distant metastasis of breast cancer. J Natl Cancer Inst *106*. 10.1093/jnci/dju136.
Rolny, C., Mazzone, M., Tugues, S., Laoui, D., Johansson, I., Coulon, C., Squadrito, M.L., Segura, I., Li, X., Knevels, E., et al. (2011). HRG inhibits tumor growth and metastasis by inducing macrophage polarization and vessel normalization through downregulation of PlGF. Cancer Cell *19*, 31-44. 10.1016/j.ccr.2010.11.009.
Roy, H., Bhardwaj, S., and Yla-Herttuala, S. (2006). Biology of vascular endothelial growth factors. FEBS Lett *580*, 2879-2887. 10.1016/j.febslet.2006.03.087.
Sheppard, V.B., Faul, L.A., Luta, G., Clapp, J.D., Yung, R.L., Wang, J.H., Kimmick, G., Isaacs, C., Tallarico, M., Barry, W.T., et al. (2014). Frailty and adherence to adjuvant hormonal therapy in older women with breast cancer: CALGB protocol 369901. J Clin Oncol *32*, 2318-2327. 10.1200/JCO.2013.51.7367.
Tacconi, C., Correale, C., Gandelli, A., Spinelli, A., Dejana, E., D'Alessio, S., and Danese, S. (2015). Vascular endothelial growth factor C disrupts the endothelial lymphatic barrier to promote colorectal cancer invasion. Gastroenterology *148*, 1438-1451 e1438. 10.1053/j.gastro.2015.03.005.
Tammela, T., Zarkada, G., Nurmi, H., Jakobsson, L., Heinolainen, K., Tvorogov, D., Zheng, W., Franco, C.A., Murtomaki, A., Aranda, E., et al. (2011). VEGFR-3 controls tip to stalk conversion at vessel fusion sites by reinforcing Notch signalling. Nat Cell Biol *13*, 1202-1213. 10.1038/ncb2331.
Ullah, I., Karthik, G.M., Alkodsi, A., Kjallquist, U., Stalhammar, G., Lovrot, J., Martinez, N.F., Lagergren, J., Hautaniemi, S., Hartman, J., and Bergh, J. (2018). Evolutionary history of metastatic breast cancer reveals minimal seeding from axillary lymph nodes. J Clin Invest *128*, 1355-1370. 10.1172/JCI96149.

Valtola, R., Salven, P., Heikkila, P., Taipale, J., Joensuu, H., Rehn, M., Pihlajaniemi, T., Weich, H., deWaal, R., and Alitalo, K. (1999). VEGFR-3 and its ligand VEGF-C are associated with angiogenesis in breast cancer. Am J Pathol *154*, 1381-1390. 10.1016/S0002-9440(10)65392-8.
Waks, A.G., and Winer, E.P. (2019). Breast Cancer Treatment: A Review. JAMA *321*, 288-300. 10.1001/jama.2018.19323.
Yang, M., McKay, D., Pollard, J.W., and Lewis, C.E. (2018). Diverse Functions of Macrophages in Different Tumor Microenvironments. Cancer Res *78*, 5492-5503. 10.1158/0008-5472.CAN-18-1367.

FIGURE LEGENDS

Figure 1. VEGF-C is highly expressed in TAMs derived from 66cl4 tumors but not 4T1 tumors.

66cl4 and 4T1 cancer cells were injected into the mammary fat pad of syngeneic mice.

(A), The graph displays the number of 66cl4 and 4T1 metastatic colonies in lungs and lymph nodes per gram of tumor weight.

(B), Fold change of the indicated genes in flow cytometry-sorted 66cl4-TAMs as compared to 4T1-TAMs, analyzed by qPCR.

(C–H), Immunofluorescence analysis of 66cl4 and 4T1 tumor sections immunoassayed for the pan-macrophage marker F4/80 (green) and cell nuclei (DAPI, grey). In (C,E,G), representative images. VEGF-C (red) in (C), LYVE-1 (red) in (E), podoplanin (red) in (G). Morphometric analysis of VEGF-C (in D), LYVE-1 (in F) and podoplanin in (H) expressing F4/80^{+} TAMs are displayed in the graphs (D,F and H).

(I-J), Confocal microscopy analysis of 66cl4 and 4T1 tumor sections showing the pan-blood vessel marker CD31 (red) and the lymph vessel marker VEGFR3 (red) and DAPI (grey). Representative images from tumor periphery in (I) and tumor inner region in (K). Morphometric analysis of VEGFR3^{+}CD31^{-} lymphatic vessel area in (J), and number VEGFR3^{+}CD31^{+} blood vessels in (L).

Statistical analyses were performed by Students t-test, stars indicate significance: *$p<0.05$, **$p<0.01$, ***$p<0.001$ and ****$p<0.0001$; n=10 mice/group; data values are presented as mean ± SD. At least 10 optical fields (OF) are visualized per tumor section and representative images are shown. Bars represent 50 µm.

Figure 2. TAM-derived VEGF-C decreases pulmonary metastasis

4T1 cancer cells were injected into the mammary fat pad of syngeneic chimeric mice harboring haemopoietic cells transduced with *Vegfc* or *Ctr* lentiviral vectors.

(A–B), immunofluorescence analysis of 4T1-*Ctr* and 4T1-*Vegfc* tumor sections for F4/80 (blue), CD45 (green), VEGF-C (red) and DAPI (grey). Representative images in (A). Morphometric analysis of VEGF-C expressing TAMs shown in (B).

(C), Graphs show tumor growth of *Ctr* and *Vegfc*-treated 4T1 tumors.

(D-E), Lymph node (D) and lung (E) colonies per tumor weight (g).

(F), Immunohistochemical analysis of MENA expressing cancer cells in lungs from tumor bearing *Ctr* and *Vegfc*-chimeric mice are depicted in the pictograms. Graph shows metastatic index [cancer cell foci/ tumor weight (g)].

(G–J), Immunofluorescence analysis of 4T1 tumor sections immunoassayed for CD31 (green), VEGFR3 (red) and DAPI (grey) in (G). Quantification of VEGFR3$^+$CD31$^+$ blood vessels in (H), % of CD31$^+$ blood vessel area in (I) and vessel number in (J).

(K–N), Immunofluorescence analysis by confocal microscopy of tumor sections immunoassayed for F4/80 (green), LYVE-1 (red) and DAPI (grey) in (K) and F4/80 (green), Podoplanin (red) and DAPI (grey) in (M). Graph depicts percentage of LYVE-1$^+$F4/80$^+$ TAMs in (L) and Podoplanin$^+$F4/80$^+$ TAMs in (N).

Statistical analyses were performed by Students t-test (**B**, **D-E,H-J** and **N-M**)and two-way ANOVA in (**C**); *p<0.05; **p<0.01, ***p<0.001 and ****p<0.001; n>12 mice/group. All data values are shown as the mean ± SD. Representative images are shown. At least 10 OFs are visualized per tumor section and representative images are shown. Bars represent 50 μm in (A, G, K and M) and 100 μm in (F). White arrows indicate double positive cells in (G, K and M) and tumor cell foci in (F).

Figure 3. VEGF-C expressing TAMs normalizes the tumor vasculature

(A–F), 4T1 tumor bearing *Ctr*-and *Vegfc*-chimeric mice were injected with FITC-lectin intravenously and PIMO intraperitoneally before sacrification. Representative images show immunostaining for CD31 (red), FITC-conjugated lectin (green) and DAPI (grey) in (A), PIMO (hypoxia) and DAPI (grey) in (C), CD31 (blue), the pericyte markers α-SMA (red) and NG2 (green), and DAPI (grey) in (E). Graph shows morphometric analysis of vessel perfusion in (B), hypoxia in (D), pericyte covered vessels in (F).

(G-L), 4T1 cancer cells were co-mingled in matrigel with BMDMs previously transduced with C*tr* or *Vegfc* LVs and injected subcutaneously into syngeneic mice. FITC-conjugated lectin and PIMO were injected before sacrification 8 days post-injection. Tumor sections were immunoassayed for CD31 (red), FITC-conjugated lectin (green) and DAPI (grey) in (G), CD31 (red), VEGFR3 (green) and DAPI (grey) in (I) PIMO (green) and DAPI (grey) in (K).

Morphometric analyses of perfused vessels are depicted in (H), VEGFR3 expressing blood vessels in (J) and hypoxic area in (L).

Statistical analyses were performed by Students t-test (A-F) and One-way ANOVA (G-L); **$p<0.01$ and ***$p<0.001$; $n>10$ mice/group. All data values are shown as the mean ± SD. At least 10 OFs are visualized per tumor section and representative images are shown. Bars represent 50 μm.

Figure 4. TAM-derived VEGF-C inversely correlates to the grade of malignancy in human breast cancer and density of TMEM

(A–C), Immunofluorescence analysis by confocal microscopy of human ER^+ breast tumors immunoassayed for CD31 (blue); pan-macrophage marker CD68 (green) and nuclei (DAPI; grey). Representative images in (A), quantitative analysis of $CD68^+$TAMs in (B) and $CD68^+$ perivascular TAMs in (C).

(D–F), Immunofluorescence analysis by confocal microscopy of human ER^+ breast tumors immunoassayed for CD31 (blue), CD68 (green), and VEGF-C (red). Representative images in (D) and quantitative analysis of VEGF-C expressing bulk TAMs in (E) and perivascular TAMs in (F).

(G-I), Representative pictograms display TMEM assembly (white arrows). Whole BC specimens were immunoassayed for CD31 (blue), CD68 (green), MENA (red) and DAPI (grey), in (G). TMEM assembly was assessed by quantifying 20 high-magnification fields/tumor section, visualized in (H), Pearson's correlation is (R^2=-0.7250, **$p<0.01$) for TMEM assembly versus VEGF-C-expressing TAMs depicted in (I).

Statistical analyses were performed by one-way ANOVA in (B,C,E and F) and by Mann-Whitney U test in (H); **$p<0.01$ ***$p<0.001$, ****$p<0.0001$; $n=4$ for grade I, $n=14$ for grade II and 10 for grade III. Data are presented as the mean ± SD. At least 20 OFs are visualized per tumor section and representative images are shown. Bars represent 100 μm in (A,D) and 20 μm in (G).

Figure 1

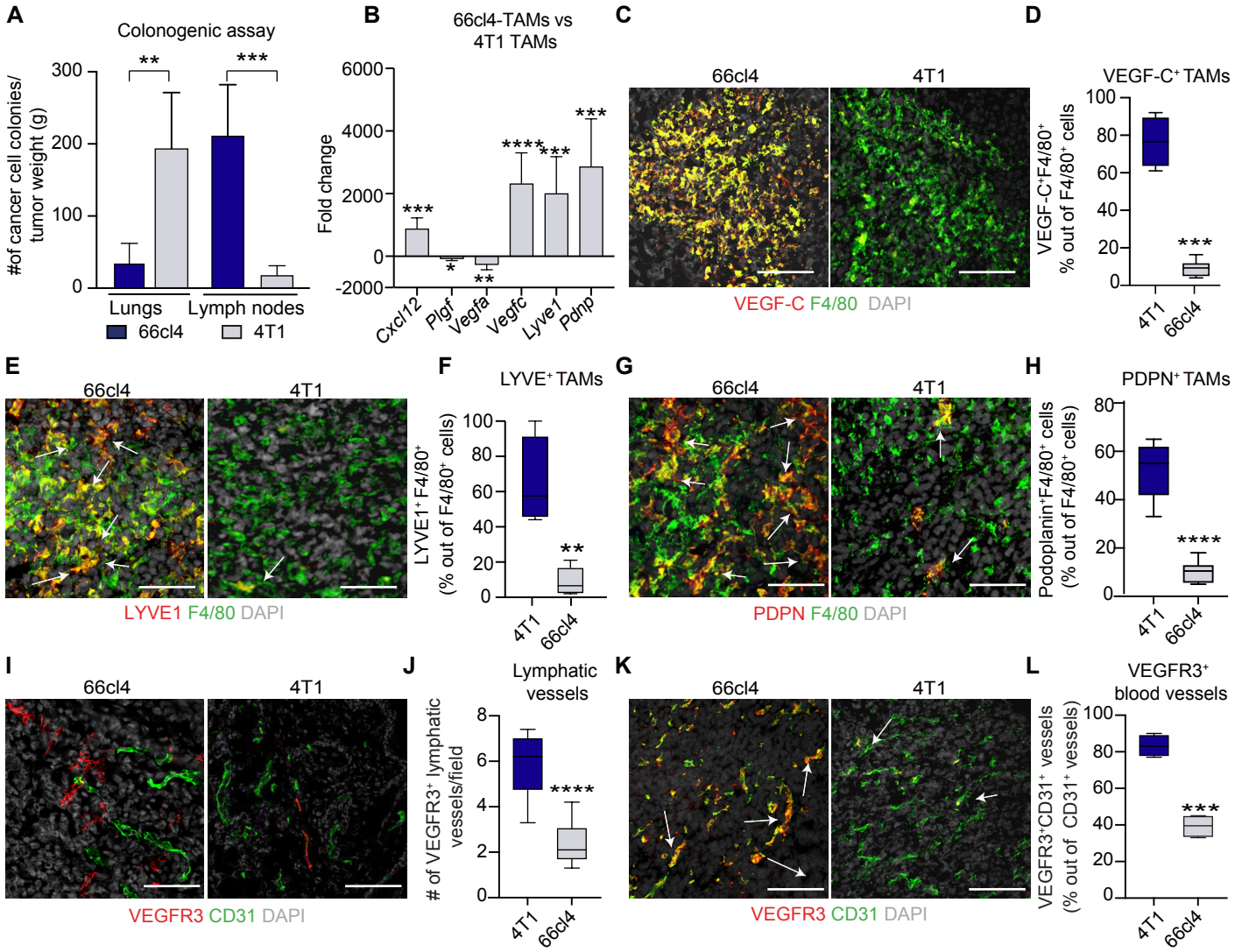
A
Colonogenic assay
#of cancer cell colonies/ tumor weight (g)
300
200
100
0
**
***
Lungs
Lymph nodes
66cl4
4T1
B
66cl4-TAMs vs 4T1 TAMs
Fold change
6000
4000
2000
0
-2000
***
*
**
****
***
***
Cxcl12
Plgf
Vegfa
Vegfc
Lyve1
Pdnp
C
66cl4
4T1
VEGF-C F4/80 DAPI
D
VEGF-C⁺ TAMs
VEGF-C⁺F4/80⁺ % out of F4/80⁺ cells
100
80
60
40
20
0
***
4T1
66cl4
E
66cl4
4T1
LYVE1 F4/80 DAPI
F
LYVE⁺ TAMs
LYVE1⁺ F4/80⁺ (% out of F4/80⁺ cells)
100
80
60
40
20
0
**
4T1
66cl4
G
66cl4
4T1
PDPN F4/80 DAPI
H
PDPN⁺ TAMs
Podoplanin⁺F4/80⁺ cells (% out of F4/80⁺ cells)
80
60
40
20
0
****
4T1
66cl4
I
66cl4
4T1
VEGFR3 CD31 DAPI
J
Lymphatic vessels
# of VEGFR3⁺ lymphatic vessels/field
8
6
4
2
0
****
4T1
66cl4
K
66cl4
4T1
VEGFR3 CD31 DAPI
L
VEGFR3⁺ blood vessels
VEGFR3⁺CD31⁺ vessels (% out of CD31⁺ vessels)
100
80
60
40
20
0
***
4T1
66cl4

Figure 2

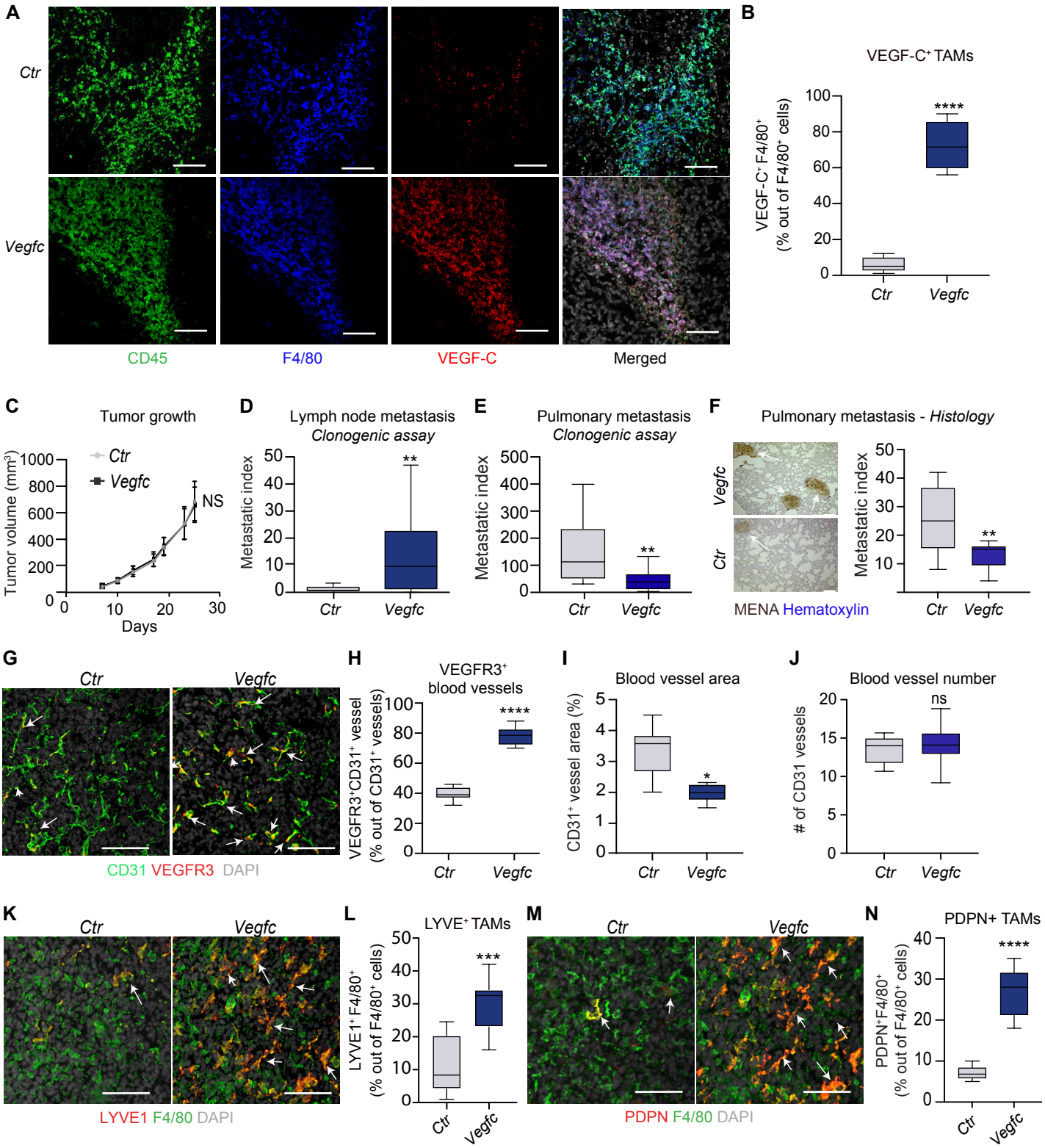
A
Ctr
Vegfc
CD45
F4/80
VEGF-C
Merged
B
VEGF-C⁺ TAMs
VEGF-C⁺ F4/80⁺ (% out of F4/80⁺ cells)
****
Ctr
Vegfc
C
Tumor growth
Tumor volume (mm³)
Ctr
Vegfc
NS
Days
D
Lymph node metastasis
Clonogenic assay
Metastatic index
**
E
Pulmonary metastasis
Clonogenic assay
Metastatic index
**
F
Pulmonary metastasis - Histology
Vegfc
Ctr
MENA Hematoxylin
Metastatic index
**
G
Ctr
Vegfc
CD31 VEGFR3 DAPI
H
VEGFR3⁺ blood vessels
VEGFR3⁺CD31⁺ vessel (% out of CD31⁺ vessels)
****
I
Blood vessel area
CD31⁺ vessel area (%)
*
J
Blood vessel number
# of CD31 vessels
ns
K
Ctr
Vegfc
LYVE1 F4/80 DAPI
L
LYVE⁺ TAMs
LYVE1⁺ F4/80⁺ (% out of F4/80⁺ cells)
***
M
Ctr
Vegfc
PDPN F4/80 DAPI
N
PDPN+ TAMs
PDPN⁺F4/80⁺ (% out of F4/80⁺ cells)
****

Figure 3

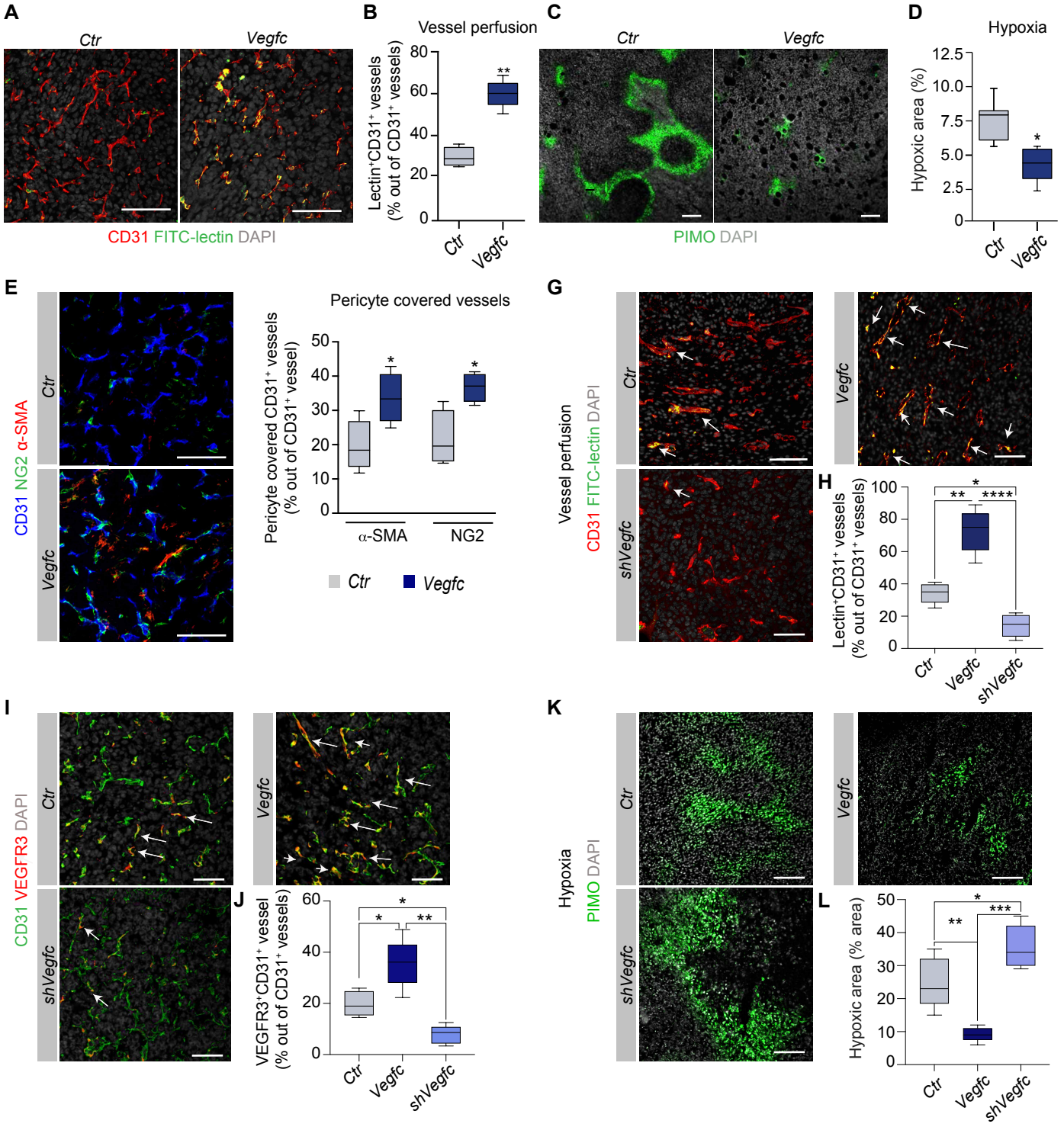
A
Ctr
Vegfc
CD31 FITC-lectin DAPI
B
Vessel perfusion
Lectin+CD31+ vessels (% out of CD31+ vessels)
80
60
40
20
0
**
Ctr
Vegfc
C
Ctr
Vegfc
PIMO DAPI
D
Hypoxia
Hypoxic area (%)
12.5
10.0
7.5
5.0
2.5
0
*
Ctr
Vegfc
E
CD31 NG2 α-SMA
Ctr
Vegfc
Pericyte covered vessels
Pericyte covered CD31+ vessels (% out of CD31+ vessel)
50
40
30
20
10
0
*
*
α-SMA
NG2
Ctr
Vegfc
G
Vessel perfusion
CD31 FITC-lectin DAPI
Ctr
Vegfc
shVegfc
H
Lectin+CD31+ vessels (% out of CD31+ vessels)
100
80
60
40
20
0
*
**
****
Ctr
Vegfc
shVegfc
I
CD31 VEGFR3 DAPI
Ctr
Vegfc
shVegfc
J
VEGFR3+CD31+ vessel (% out of CD31+ vessels)
60
40
20
0
*
*
**
Ctr
Vegfc
shVegfc
K
Hypoxia
PIMO DAPI
Ctr
Vegfc
shVegfc
L
Hypoxic area (% area)
50
40
30
20
10
0
*
**
***
Ctr
Vegfc
shVegfc

Figure 4

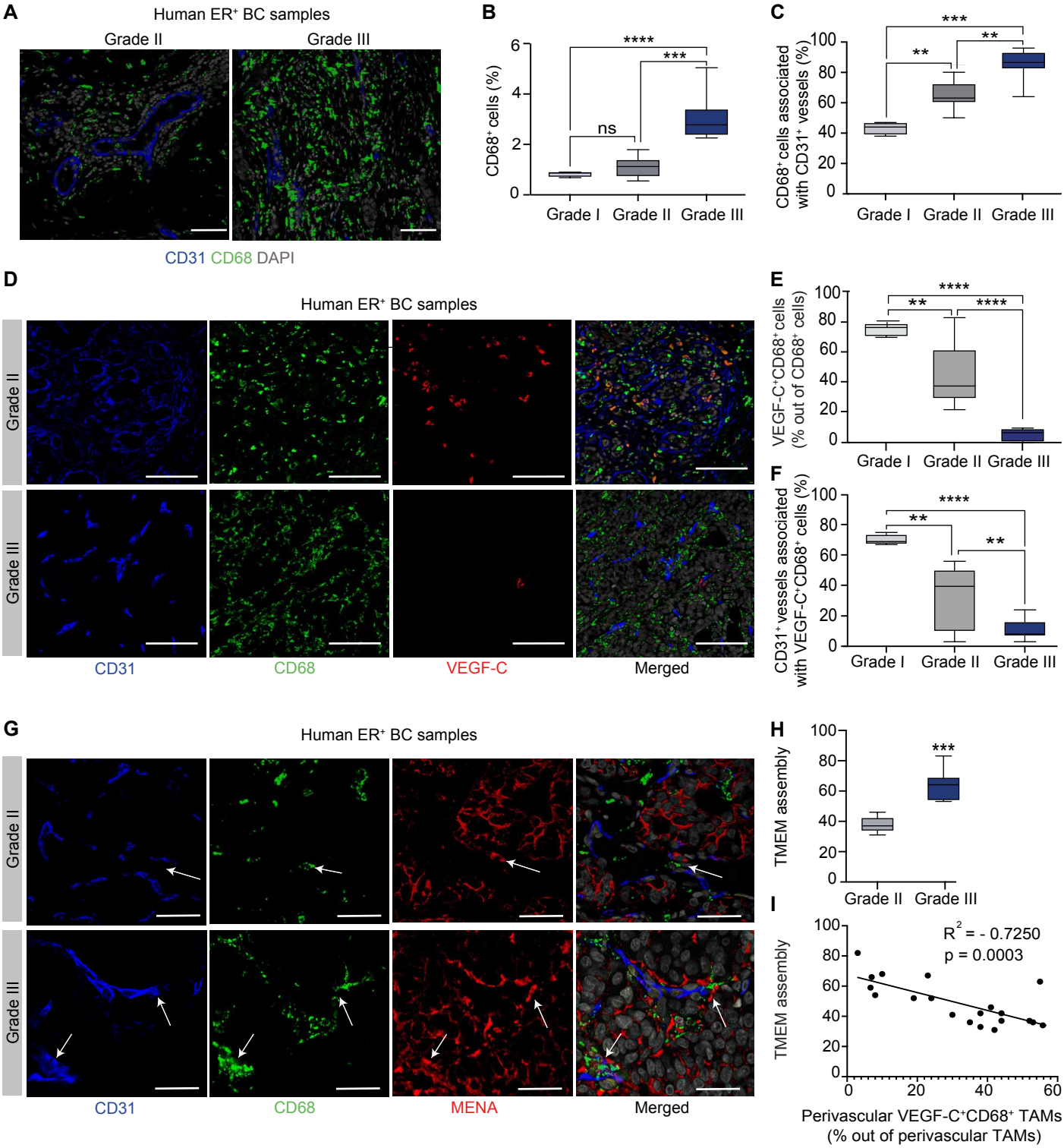
A
Human ER+ BC samples
Grade II
Grade III
CD31 CD68 DAPI
B
CD68+ cells (%)
****
***
ns
Grade I
Grade II
Grade III
C
CD68+ cells associated with CD31+ vessels (%)
***
**
**
Grade I
Grade II
Grade III
D
Human ER+ BC samples
Grade II
Grade III
CD31
CD68
VEGF-C
Merged
E
VEGF-C+CD68+ cells (% out of CD68+ cells)
****
**
****
Grade I
Grade II
Grade III
F
CD31+ vessels associated with VEGF-C+CD68+ cells (%)
****
**
**
Grade I
Grade II
Grade III
G
Human ER+ BC samples
Grade II
Grade III
CD31
CD68
MENA
Merged
H
TMEM assembly
***
Grade II
Grade III
I
TMEM assembly
R2 = - 0.7250
p = 0.0003
Perivascular VEGF-C+CD68+ TAMs
(% out of perivascular TAMs)